

Energy & Environmental Science

Accepted Manuscript



This is an *Accepted Manuscript*, which has been through the Royal Society of Chemistry peer review process and has been accepted for publication.

Accepted Manuscripts are published online shortly after acceptance, before technical editing, formatting and proof reading. Using this free service, authors can make their results available to the community, in citable form, before we publish the edited article. We will replace this *Accepted Manuscript* with the edited and formatted *Advance Article* as soon as it is available.

You can find more information about *Accepted Manuscripts* in the [Information for Authors](#).

Please note that technical editing may introduce minor changes to the text and/or graphics, which may alter content. The journal's standard [Terms & Conditions](#) and the [Ethical guidelines](#) still apply. In no event shall the Royal Society of Chemistry be held responsible for any errors or omissions in this *Accepted Manuscript* or any consequences arising from the use of any information it contains.

Na_{0.67}Mn_{1-x}Mg_xO₂ (0 ≤ x ≤ 0.2): A High Capacity Cathode for Sodium-Ion Batteries

Cite this: DOI: 10.1039/x0xx00000x

Juliette Billaud,^a Gurpreet Singh,^b A. Robert Armstrong,^a Elena Gonzalo,^b Vladimir Roddatis,^b Michel Armand,^b Teófilo Rojo^b and Peter G. Bruce^a

Received 00th January 2012,
Accepted 00th January 2012

DOI: 10.1039/x0xx00000x

www.rsc.org/

Earth-abundant Na_{0.67}[Mn_{1-x}Mg_x]O₂ (0 ≤ x ≤ 0.2) cathode materials with the P2 structure have been synthesized as positive electrodes for sodium-ion batteries. Na_{0.67}MnO₂ exhibits a capacity of 175 mAh g⁻¹ with good capacity retention. A Mg content of 5 % is sufficient to smooth the charge/discharge profiles without affecting the capacity, whilst further increasing the Mg content improves the cycling stability, but at the expense of a lower discharge capacity (~150 mAh g⁻¹ for Na_{0.67}Mn_{0.8}Mg_{0.2}O₂). It was observed that the cooling process during synthesis, as well as Mg content, have an influence on the structure.

Lithium-ion batteries have dominated the world of portable electronic devices over the past two decades and are making their way into the electric vehicle market due to their high energy density.¹ However, recently sodium ion batteries have regained the interest of the scientific community due to the high and uniform abundance of sodium across the world and consequent low cost compared to lithium.²⁻⁷ Various electrode materials have been studied for sodium batteries. Due to the similarity in the operation of lithium and sodium ion batteries, sodium equivalents of the lithium based electrode materials, such as hard carbon, phosphates, pyrophosphates, oxides and oxyanions, have been studied.⁸⁻¹⁰ Layered oxides, AMO₂, where A = Li, Na and M is one or more transition metals, exhibit very different behavior depending on the alkali ion. For example, electrochemically inactive LiFeO₂ and LiCrO₂ behave well in their sodium forms, NaFeO₂ and NaCrO₂, due to the accessibility of the Fe⁴⁺ and Cr⁴⁺ states when A = Na.¹¹⁻¹³

The main market for Na-ion batteries is in grid-scale storage, where cost is of paramount importance, thus attention is focused on sodium cathodes based on low-cost, earth-abundant, transition metals such as Mn and Fe. Here we show that Na_{0.67}MnO₂ with the P2 structure (Fig. 1) exhibits a high capacity (175 mAh g⁻¹) with good capacity retention, in contrast to a previous study where the capacity faded rapidly.¹⁴ This improvement could be explained by the use of a different synthesis route as well as an improved electrolyte. Good

cyclability was also recently reported for this material by Su et al.¹⁵ Moreover, the capacity is only 15 mAh g⁻¹ lower than the highest capacity reported for a low-cost Na oxide cathode, Na_{0.67}[Fe_{1/2}Mn_{1/2}]O₂.¹⁶ Due to the presence of Jahn–Teller active Mn³⁺ in Na_{0.67}MnO₂, the structure undergoes various structural transitions during sodiation/desodiation.¹⁴⁻¹⁷ This leads to many voltage steps in the charge/discharge profile, which may be a handicap for practical implementation of such materials.¹⁸ A very recent study has shown that the crystal structure may be stabilized by substituting Mn by Co, but at the expense of a large decrease in the charge/discharge capacity. Moreover, Co is expensive, toxic and its use is incompatible with the philosophy driving towards sodium batteries.¹⁷ Instead, we have investigated reducing the phase transitions by substituting Mn³⁺ ions with Mg²⁺ ions (Na_{0.67}[Mn_{1-x}Mg_x]O₂ with 0 ≤ x ≤ 0.2), which have a strong preference for octahedral sites in the layered oxide framework. This leads to the formation of a highly stable framework that shows a smooth charge/discharge profile with low polarization (lower than Na_{0.67}[Fe_{1/2}Mn_{1/2}]O₂) and a capacity of ~175 mAh g⁻¹ (Fig. 2 and Fig. 3). Such an observation is significant for the future development of sodium ion battery cathode materials.

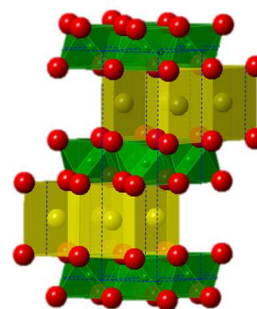


Fig. 1. Schematic representation of the ideal P2 structure. NaO₆ trigonal prisms (yellow), MO₆ octahedra (green) and oxygen (red).

All materials were prepared and cells assembled as described in the Experimental Section in the Supporting Information.

Powder XRD patterns of $\text{Na}_{0.67}\text{Mn}_{1-x}\text{Mg}_x\text{O}_2$, where $x = 0.0, 0.05, 0.1$ and 0.2 are shown in Fig. 4. Lattice parameters of all the substituted compositions could be refined using hexagonal ($P6_3/mcm$) and orthorhombic ($Cmcm$) space group symmetries, whilst the situation pertaining to $\text{Na}_{0.67}\text{MnO}_2$ samples proved more complex. The ideal P2 structure, Fig. 1, has hexagonal symmetry, ($P6_3/mcm$). X-ray diffraction measurements on $\text{Na}_{0.67}\text{MnO}_2$, prepared by quenching show the formation of an orthorhombic phase (space group $Cmcm$) representing an $a \times \sqrt{3} a \times c$ superstructure of the basic hexagonal unit cell (the additional reflections associated with this superstructure are indicated in Fig. 4) together with the presence of a very similar monoclinic phase (space group $C2/n$, Fig. 4), in agreement with the earlier reported literature.¹⁹ Under slow cooling conditions the simple hexagonal phase (space group $P6_3/mcm$) predominates, with around 20 % of the monoclinic phase present.²⁰ The lattice parameters and phase fractions for all the phases studied are summarized in Table 1. The deviation from an ideal hexagonal phase is due to the presence of the Jahn-Teller active Mn^{3+} ion.¹⁹ Slow cooling leads to the presence of manganese vacancies thus a higher concentration of Mn^{4+} which suppresses the cooperative Jahn-Teller distortion. Therefore leading to the stabilisation of the undistorted (ideal) P2 hexagonal crystal structure.²¹ It is observed that substitution of Mn by Mg in $\text{Na}_{0.67}\text{Mn}_{1-x}\text{Mg}_x\text{O}_2$ also suppresses the orthorhombic distortion, by increasing the average Mn oxidation state closer to 4+ and by dilution of Mn^{3+} centers. This suppression is more pronounced when the doped samples are also slowly cooled, since both substitution and vacancy formation work together to reduce the Mn^{3+} content, which leads to formation of an essentially single phase undistorted hexagonal material even for $x = 0.05$, Table 1. The orthorhombic superstructure was observed for the quenched materials with $x = 0.05$ and 0.1 , whilst the quenched material with $x = 0.2$ was best described by the simple hexagonal phase. Profile fits to synchrotron X-ray diffraction data for $x = 0.1$ are presented in figure S1, with crystallographic data in Table S1. Evidently, the phase behavior is complex and varies with Mg content and synthesis conditions. Further detailed studies are underway in order to understand these changes and their influence on the electrochemistry. Such studies are beyond the scope of the present communication, which aims to report the gross features and performance of the Mg-doped $\text{Na}_{0.67}\text{MnO}_2$.

Table 1. Refined lattice parameters of various compositions of $\text{Na}_{0.67}\text{Mn}_{1-x}\text{Mg}_x\text{O}_2$ ($0 \leq x \leq 0.2$).

	x = 0		x = 0.05	x = 0.1	x = 0.2	
	<i>Cmcm</i> (70 %)	<i>C2/n</i> (30 %)	<i>Cmcm</i>	<i>Cmcm</i>	<i>P6₃/mcm</i>	
Quench	<i>a</i> /Å	2.8368(2)	2.8342(7)	2.8491(2)	2.8582(2)	2.9162(12)
	<i>b</i> /Å	5.3153(4)	5.2669(8)	5.2496(2)	5.1982(3)	2.9162(12)
	<i>c</i> /Å	11.154(1)	11.230(1)	11.187(1)	11.1980(9)	11.209(9)
	β /°		90.78(2)			
Slow Cool		<i>P6₃/mcm</i> (80 %)	<i>C2/n</i> (20 %)	<i>P6₃/mcm</i>	<i>P6₃/mcm</i>	
	<i>a</i> /Å	2.8818(2)	2.828(2)	2.8856(3)	2.9008(5)	2.8988(4)
	<i>b</i> /Å	2.8818(2)	5.287(1)	2.8856(3)	2.9008(5)	2.8988(4)
	<i>c</i> /Å	11.156(2)	11.204(5)	11.144(3)	11.218(2)	11.224(2)
	β /°		91.04(4)			

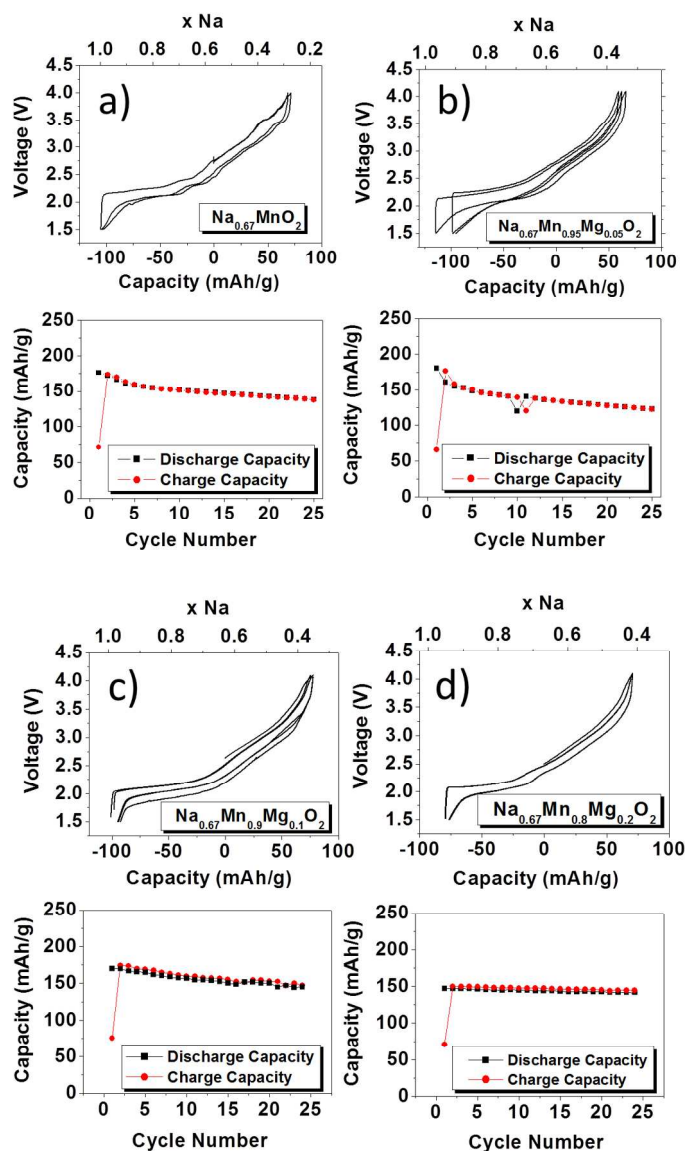


Fig. 2. Electrochemical charge/discharge curves along with cycling performance up to 25 cycles for slow-cooled (a) $\text{Na}_{0.67}\text{MnO}_2$, (b) $\text{Na}_{0.67}\text{Mn}_{0.95}\text{Mg}_{0.05}\text{O}_2$ (c) $\text{Na}_{0.67}\text{Mn}_{0.9}\text{Mg}_{0.1}\text{O}_2$ and (d) $\text{Na}_{0.67}\text{Mn}_{0.8}\text{Mg}_{0.2}\text{O}_2$. Cycling commenced on charge. The rate was 12 mA g^{-1} .

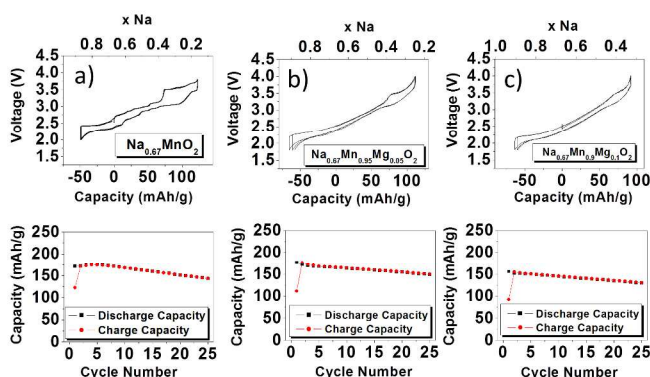


Fig. 3. Electrochemical charge/discharge curves along with cycling performance up to 25 cycles for quenched (a) $\text{Na}_{0.67}\text{MnO}_2$, (b) $\text{Na}_{0.67}\text{Mn}_{0.95}\text{Mg}_{0.05}\text{O}_2$ and (c) $\text{Na}_{0.67}\text{Mn}_{0.9}\text{Mg}_{0.1}\text{O}_2$. Cycling commenced on charge. The rate was 12 mA g^{-1} .

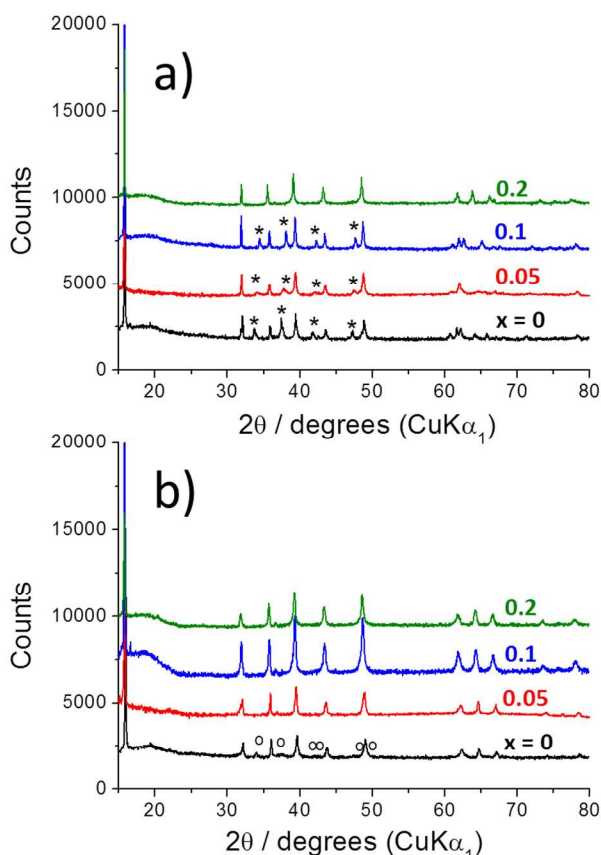


Fig. 4 Powder X-ray diffraction patterns of $\text{Na}_{0.67}\text{Mn}_{1-x}\text{Mg}_x\text{O}_2$ for (a) quenched and (b) slow cooled samples. Values of x are shown in the plots. The $a \times \sqrt{3} a \times c$ superlattice peaks in the quenched materials are represented by the symbol *, peaks from the monoclinic phase are weak and overlap with the superlattice peaks. In the slow cooled samples, the peaks related to the monoclinic $C2/n$ phase are represented by the symbol °. The hump at $2\theta \approx 20^\circ$ corresponds to Kapton® film.

Typical electrochemical charge/discharge profiles of slow-cooled and quenched $\text{Na}_{0.67}\text{Mn}_{1-x}\text{Mg}_x\text{O}_2$ are shown in Figs. 2 and 3, respectively. In all cases, undoped and Mg-doped samples (independent of the cooling regime) sustained cycling, which is indicative of good stability. Capacity retention for quenched $\text{Na}_{0.67}\text{Mn}_{0.95}\text{Mg}_{0.05}\text{O}_2$ up to 50 cycles is shown in Fig. S2. Consistently, Mg doping results in a smoothing of the load curve, although this effect is more pronounced in the case of the quenched materials.

A particularly significant phase transition is evident as a plateau above 3.5V vs. Na^+/Na , Figs. 2 and 3. It is identified as the transition between the P2 structure and the OP4 phase, which shows an alternate stacking of octahedral and trigonal prismatic layers along the c -axis, as has been reported previously in $\text{Na}_{0.67}[\text{Fe}_{1/2}\text{Mn}_{1/2}]\text{O}_2$.¹⁶ This transition is especially evident in quenched $\text{Na}_{0.67}\text{MnO}_2$ and $\text{Na}_{0.67}\text{Mn}_{0.95}\text{Mg}_{0.05}\text{O}_2$, Fig. 3, where it was confirmed to be the P2-OP4 transition by powder X-ray diffraction at the end of charge (Fig. 5). The absence of any X-ray signature for the plateaus in slow cooled $x = 0, 0.05$ and 0.1 samples at the end of charge, Fig. 5, is in accord with the much smaller extent of the plateaus for these compositions, Figs 2 and 3, and may reflect the fact that small nuclei of the OP4 phase forming as P2 begins to transform to OP4 are sufficient to impact on the energetics and hence voltage features, even if they do not result in long range order and diffraction. The deleterious effect of the phase transition is most clearly seen in the undoped materials, where the transition is prominent in the quenched material resulting in a larger polarization and somewhat greater capacity fade compare with the slow-cooled material for which the transition is much less prominent.

The main trend with increasing Mg content for the slow-cooled materials, in addition to smoothing the charge/discharge curves, is a gradual reduction in the initial capacity and improvement in the capacity retention. In the case of the quenched materials the capacity is again reduced but with less effect on the capacity retention.

The smoother charge/discharge profiles in the Mg substituted materials may, in part, be explained on the basis of replacing 2 high spin Mn^{3+} ions with 1 Mg^{2+} and 1 Mn^{4+} leading to fewer Jahn–Teller active ions. The increased amount of Mn^{4+} associated with both Mg substitution and also slow cooling leads to a reduction in the initial discharge capacity as shown in Figs. 2 and 3. Furthermore magnetic measurements reveal a reduction in magnetic moment from $4.49 \mu_B$ $\text{Na}_{0.67}\text{MnO}_2$ to $3.71 \mu_B$ for $\text{Na}_{0.67}\text{Mn}_{0.8}\text{Mg}_{0.2}\text{O}_2$ consistent with a higher proportion of Mn^{4+} . On replacing 0.05 Mn by Mg the theoretical capacity is reduced from 244 to 227 mAh g^{-1} due to the presence of the electrochemically inactive Mg in the crystal structure, but this does not generate a reduction of the initial discharge capacity in the substituted samples since we observe 175 mAh g^{-1} for $\text{Na}_{0.67}\text{Mn}_{0.95}\text{Mg}_{0.05}\text{O}_2$. The substitution limit for the replacement of Mn by Mg in $\text{Na}_{2/3}\text{Mn}_{1-x}\text{Mg}_x\text{O}_2$ is observed to be $x = 0.25$ (synthesized at $\sim 1000^\circ\text{C}$), even though the theoretical limit, corresponding to all Mn in +4 oxidation state is 0.33.¹⁹ This may be due to the tendency of the Mn to adopt lower oxidation states at higher temperatures (synthesis was at 900°C). At these higher degrees of substitution the voltage profiles continue to be smooth, as expected, and the capacity retention is excellent. For example, $\text{Na}_{0.67}\text{Mn}_{0.8}\text{Mg}_{0.2}\text{O}_2$ in Fig. 2 (d) exhibits an initial discharge capacity of $\sim 150 \text{ mAh g}^{-1}$ close to the theoretical capacity (167 mAh g^{-1} assuming no Mn vacancies), with a capacity retention of 96 % after 25 cycles.

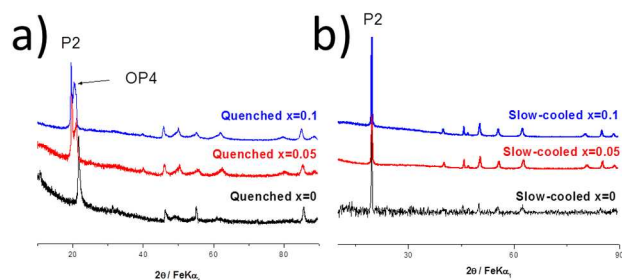


Fig 5. Powder XRD patterns at the end of charge for quenched ($x = 0, 0.05$ and 0.1) (a) and slow cooled ($x = 0, 0.05$ and 0.1) $\text{Na}_{0.67}\text{Mn}_{1-x}\text{Mg}_x\text{O}_2$ (b).

Microstructural characterisation was performed on the powder samples and corresponding micrographs of the various compositions are shown in Fig. 5. The morphology of $\text{Na}_{0.67}\text{MnO}_2$, $\text{Na}_{0.67}\text{Mn}_{0.95}\text{Mg}_{0.05}\text{O}_2$, $\text{Na}_{0.67}\text{Mn}_{0.9}\text{Mg}_{0.1}\text{O}_2$ and $\text{Na}_{0.67}\text{Mn}_{0.8}\text{Mg}_{0.2}\text{O}_2$ powders depicted in Fig. 4 (a), (b), (c) and (d) respectively, show well-formed plate-like crystals especially the samples with higher Mg-content. The diameter of these plates is 3 – 4 μm with a thickness in the submicron range. The composition of samples prepared in the form of pellets was verified by EDX,²² and was found to lie within 2 % of expected values. The distribution of all elements was uniform as observed by EDX mapping.

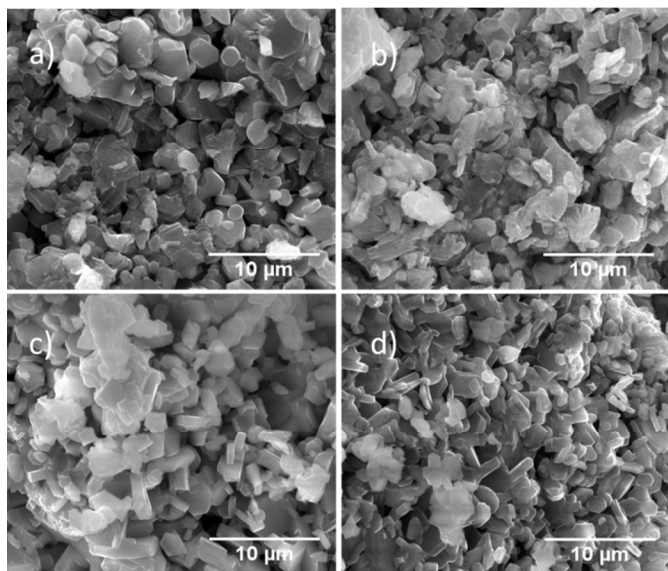


Fig. 6 SEM images of (a) $\text{Na}_{0.67}\text{MnO}_2$ (b) $\text{Na}_{0.67}\text{Mn}_{0.95}\text{Mg}_{0.05}\text{O}_2$ (c) $\text{Na}_{0.67}\text{Mn}_{0.9}\text{Mg}_{0.1}\text{O}_2$ and (d) $\text{Na}_{0.67}\text{Mn}_{0.8}\text{Mg}_{0.2}\text{O}_2$ powder samples.

Conclusions

In conclusion the charge/discharge profile of $\text{Na}_{0.67}\text{MnO}_2$ has been smoothed, the polarization reduced and the capacity retention improved by substitution of Mn with Mg in this cathode material for Na-ion batteries. The discharge capacity is 175 mAh g^{-1} for $\text{Na}_{0.67}\text{Mn}_{0.95}\text{Mg}_{0.05}\text{O}_2$. Such behavior in a sodium-ion battery cathode material based on Earth abundant Mg, Mn and Na, layered oxides and prepared by a

straightforward synthesis, is very encouraging for the future development of NIBs.

Notes and references

^a School of Chemistry, University of St. Andrews, St. Andrews, Fife KY16 9ST, UK.

^b CIC ENERGIGUNE, Parque Tecnológico de Álava, Albert Einstein 48, ED. CIC, 01510 Miñano, Spain.

† We thank Dr. Paul Adamson for his assistance in obtaining the synchrotron data. We also thank EPSRC for funding.

Electronic Supplementary Information (ESI) available: Experimental details, structure refinements and electrochemical data. See DOI: 10.1039/c000000x/

- M. Armand and J.M Tarascon, *Nature*, 2008, **451**, 652; N.-S. Choi, Z. Chen, S.A. Freunberger, G. Yushin, X. Ji, Y.-K. Sun, K. Amine, L.F. Nazar, J. Cho, P.G. Bruce, *Angew. Chem. Int. Ed.*, 2012, **51**, 9994.
- S-W. Kim, D-H Seo, X. Ma, G. Ceder and K. Kang, *Advanced Energy Materials*, 2012, **2**, 710.
- B. L. Ellis and L. F. Nazar, *Current Opinion in Solid State and Materials Science*, 2012, **16**, 168.
- V. Palomares, P. Serras, I. Villaluenga, K. B. Hueso, J. C. González, and T. Rojo, *Energy Environ. Sci.*, 2012, **5**, 5884; V. Palomares, M. C. Cabanas, E. C. Martínez, M. H. Han and T. Rojo, *Energy Environ. Sci.*, 2013, **6**, 2312.
- H. Pan, Y.-S. Hu and L. Chen, *Energy Environ. Sci.*, 2013, **6**, 2338
- M. D. Slater, D. Kim, E. Lee, C. S. Johnson, *Adv. Funct. Mater.*, 2013, **23**, 947.
- A. Ponrouch, E. Marchante, M. Courty, J.-M. Tarascon and M. R. Palacin, *Energy Environ. Sci.*, 2012, **5**, 8572.
- S. Komaba, W. Murata, T. Ishikawa, N. Yabuuchi, T. Ozeki, T. Nakayama, A. Ogata, K. Gotoh and K. Fujiwara, *Advanced Functional Materials*, 2011, **21**, 3859.
- C. Masquelier, and L. Croguennec, *Chem. Rev.*, 2013, **113**, 6552
- B. Mortemard de Boisse, D. Carlier, M. Guignard, and C. Delmas, *J. Electrochem. Soc.*, 2013, **160**, A569.
- Y. Takeda, K. Nakahara, M. Nishijima, N. Imanishi and O. Yamamoto, *Materials Research Bulletin*, 1994, **29**, 659.
- S. Komaba, C. Takei, T. Nakayama, A. Ogata and N. Yabuuchi, *Electrochem. Commun.*, 2010, **12**, 355.
- A. Mendiboure, C. Delmas and P. Hagenmuller, *J. Solid State Chem.*, 1985, **57**, 323.
- A. Caballero, L. Hernan, J. Morales, L. Sanchez, J. Santos Pena and M. A. G. Aranda, *J. Mater. Chem.*, 2002, **12**, 1142.
- D. Su, C. Wang, H.-J. Ahn and G. Wang, *Chem. Eur. Journal*, 2013, **19**, 10884.
- N. Yabuuchi, M. Kajiyama, J. Iwatate, H. Nishikawa, S. Hitomi, R. Okuyama, R. Usui, Y. Yamada and S. Komaba, *Nature Mater.*, 2012, **11** 512.
- X.F. Wang, M. Tamaru, M. Okubo and A. Yamada, *J. Phys. Chem. C*, 2013, **117**, 15545.
- D. Yuan, W. He, F. Pei, F. Wu, Y. Wu, J.-F. Qian, Y.-L. Cao, X.-P. Ai and H. Yang, *J. Mater. Chem A*, 2013, **1**, 3895.

Journal Name

- 19 R. Stoyanova, D. Carlier, M. Sendova-Vassileva, M. Yoncheva, E. Zhecheva, D. Nihtianova and C. Delmas, *J. Solid State Chem.*, 2010, **183**, 1372.
- 20 J. M. Paulsen and J. R. Dahn, *Solid State Ionics*, 1999 **126**, 3.
- 21 J.P. Parant, R. Olazcuaga, M. Devalette, C. Fouassier and P. Hagenmuller, *J. Solid State Chem.*, 1971, **3**, 1.
- 22 M. Casas-Cabanas, V. Roddatis, D. Saurel, P. Kubiak, J. Carretero, V. Palomares, P. Serras, T. Rojo, *J. Mater. Chem.*, 2012, **22**, 17421.